Moments of fusion-barrier distributions

K. E. Rehm, H. Esbensen, C. L. Jiang, B. B. Back, A. M. Stefanini, and G. Montagnoli

Phys. Rev. C **94**, 044612 — Published 18 October 2016

DOI: 10.1103/PhysRevC.94.044612

Moments of Fusion-Barrier Distributions

K.E. Rehm,[1] H. Esbensen,[1] C.L. Jiang,[1] B.B. Back,[1] A.M. Stefanini,[2] and G. Montagnoli[3]

[1]*Physics Division, Argonne National Laboratory, Argonne, Illinois 60439, USA*
[2]*INFN, Laboratori Nazionali di Legnaro, I-35020 Legnaro (Padova), Italy*
[3]*Dipartimento di Fisica e Astronomia, Universitá di Padova, and INFN, Sez. di Padova, I-35131 Padova, Italy*

A study of fusion barrier distributions through an analysis of their moments is presented. The moments can be obtained from least-squares fits of the energy-weighted fusion cross sections without the need of calculating second derivatives. The zeroth and first moment determines the fusion radius R and the Coulomb barrier V_C. These two quantities are the same as the parameters R and V_C that are used in the well-known expression, $E\sigma = \pi R^2(E - V_C)$ for the fusion cross section at high energies. The second and third moments M_2 and M_3 determine the width and skewness of the barrier distribution, respectively. From these global parameters new correlations for the study of heavy-ion induced fusion reactions can be obtained. Systems exhibiting a large coupling to transfer reactions show a small fusion radius as well as a large second moment. A negative third moment is correlated with a prolate deformation of the target nucleus.

PACS numbers: 25.70.Jj, 97.10.Cv, 97.10.Tk

I. I. INTRODUCTION

Heavy-ion fusion reactions [1, 2] have been studied extensively since fusion enhancement was discovered more than 30 years ago. It was soon realized that the fusion enhancement is caused by couplings to other reaction channels and can be described within the framework of Coupled-Channels (CC) calculations [3]. The coupling to other reaction channels leads to a multidimensional barrier, resulting for most cases in an enhanced tunneling probability [4]. Following a recipe of Balantekin et al. [5] who used barriers with a fixed height but different shapes, Stelson [6] analyzed fusion excitation functions assuming the existence of more than one barrier.

A major step forward was taken by Rowley *et al.* [7], who found that the distribution of barriers $D(E)$ can be extracted from a precise measurement of the fusion excitation function through the equation:

$$D(E) = \frac{1}{\pi R^2}\frac{d^2(E\sigma)}{dE^2}, \quad \text{with} \quad \int D(E)dE = 1. \qquad (1)$$

The barrier distribution $D(E)$ is normalized so that the total probability of encountering a barrier is 1.

Many barrier distributions have been studied by analyzing the second derivative of the energy weighted cross sections, $\frac{d^2(E\sigma)}{dE^2}$ [7, 8]. This method, however, requires fusion excitation functions with small uncertainties measured in small energy steps which are not always available. Especially at higher energies the second derivative is sometimes difficult to extract from the experimental data (see e.g. Ref. [9]) .

In this contribution we describe an analysis of fusion excitation functions by using the moments of the barrier distributions which are obtained from a plot of $E\sigma$ vs. E. The moment analysis provides global parameters and is not supposed to substitute the information contained in the individual barrier distributions. However, it is useful for a quantitative comparison of barrier distributions measured for different fusion systems. Furthermore, since they don't require the calculation of a second derivative they can be obtained from excitation functions which have been measured in larger energy steps.

II. II. MOMENTS OF BARRIER DISTRIBUTIONS

The zeroth moment of the barrier distribution $D(E)$, is the normalization condition in Eq. (1), from which the area πR^2 is obtained where R is the so-called fusion radius (see e.g. Ref. [10]):

$$\pi R^2 = \int^{E_h} \frac{d^2(E\sigma)}{dE^2}\, dE = \frac{d(E\sigma)}{dE}|_{E_h}. \qquad (2)$$

The result is a function of the upper limit E_h of the integration, whereas the contribution from the lower limit vanishes. In fact, if the lower limit is taken at the lowest experimental energy, the correction from the lower limit is typically less than 1/1000 of πR^2. The limit E_h must lie in the linear region in a plot of σE vs E.

The first moment M_1 of the barrier distribution, defined as

$$M_1 = \int^{E_h} ED(E)dE, \qquad (3)$$

is the average Coulomb barrier. By introducing the asymptotic value of $E\sigma$ which at high energies can be described by the well-known function [10]:

$$\begin{aligned} E\sigma = \pi R^2(E - V_C), \quad &\text{at} \quad E > V_C, \\ = 0, \quad &E <= V_C, \end{aligned} \qquad (4)$$

and inserting the asymptotic part of this function, the first moment of $D(E)$ can be calculated with partial in-

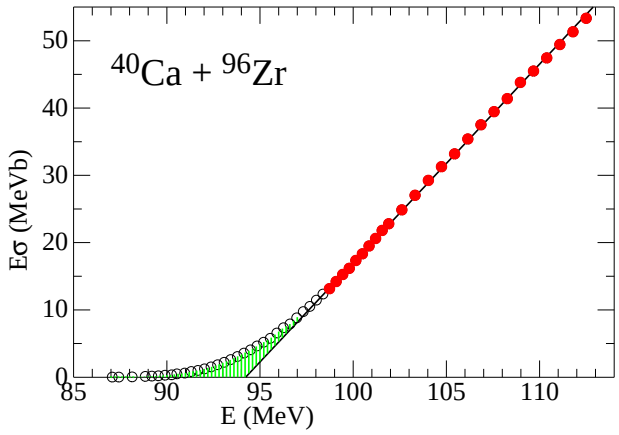

FIG. 1: (Color online) Plot of $E\sigma$ vs E for the fusion reaction ^{40}Ca + ^{96}Zr. The black line is given by the equation $\pi R^2(E - V_C)$ with parameters R and V_C obtained from a least-squares fit to the data $E > 1.04V_c$ (red circles). The second and third moments M_2 and M_3 are calculated from the green-shaded area. See text for details.

tegration and expressed as a function of the upper integration limit. One finally obtains

$$M_1 = \frac{1}{\pi R^2}\Big(E\frac{d(E\sigma)}{dE} - E\sigma\Big)|_{E_h}$$
$$= \frac{1}{\pi R^2}\Big(E\pi R^2 - \pi R^2(E - V_C)\Big)|_{E_h} = V_C. \quad (5)$$

Higher moments are defined as

$$M_n = \int^{E_h} (E - M_1)^n D(E)dE, \quad \text{for} \quad n > 1. \quad (6)$$

where $D(E)$ is the normalized barrier distribution from Eq. (1). By using partial integrations, neglecting the small corrections from the lower limit of the integration, and expressing the result in terms of the upper limit E_h one obtains

$$M_n = \frac{n(n-1)}{\pi R^2}\int^{E_h} (E - M_1)^{n-2} E\sigma dE$$
$$-(n-1)(E_h - M_1)^n. \quad (7)$$

For the second and third moments this results in:

$$M_2 = \frac{2}{\pi R^2}\int^{E_h} E\sigma dE - (E_h - V_C)^2, \quad (8)$$

and

$$M_3 = \frac{6}{\pi R^2}\int^{E_h} (E - V_C)E\sigma dE - 2(E_h - V_C)^3, \quad (9)$$

which describe the variance of the barrier distribution and its skewness, respectively.

Moments involving energy-weighted cross sections have been discussed in two earlier publications [9, 11]. While Ref. [11] discussed moments of the angular momentum, in Ref. [9] an analysis using energy-dependent moments defined as

$$K_n(E) = n(n-1)\int_0^E (E - E')^{n-2} E'\sigma(E')dE',$$
$$\text{for} \quad n \geq 2 \quad (10)$$

was proposed. As pointed out in Ref. [11], however, these moments are not directly related to observables, making it difficult to provide a physical interpretation.

TABLE I: Comparison of the parameters R, M_1, M_2 and M_3 (column 2, 3, 4, 5) obtained for the system ^{40}Ca + ^{96}Zr using all data (line 1), 1/2 of the data (line 2), *etc.* The numbers in the parentheses are the data points included in the fitting procedure using Eq. (4).

number of data	R	M_1	M_2	M_3
(used in fit)	fm	MeV	MeV^2	MeV^3
56 (25)	9.72 ±0.02	94.28 ±0.02	9.1 ±0.2	-4.7 ±1.1
29 (16)	9.65 ±0.02	94.14 ±0.02	8.4 ±0.2	-6.3 ±0.6
20 (11)	9.61 ±0.03	94.08 ±0.03	8.2 ±0.2	-4.2 ±0.8
15 (8)	9.62 ±0.03	94.10 ±0.03	8.4 ±0.3	-0.9 ±1.2

In order to show how the moments defined in Eqs. (2, 3, 6) are extracted from the data, experimental results of ^{40}Ca + ^{96}Zr (Ref. [12, 13]) are presented in Fig. 1. The circles represent the measured values $E\sigma$. The solid line is given by the function $\pi R^2(E - V_C)$ obtained from a least-squares fit to the solid circles, which describes the behavior of $E\sigma$ at higher energies. From the slope one obtains the value πR^2, which describes the average of the derivative $d(E\sigma)/dE$ at high energies. The crossing point of this line with the x-axis gives the first moment M_1 *i.e.* the Coulomb barrier V_C. This method for extracting V_C and πR^2 has been discussed in the past by many authors (see *e.g.* Ref. [10] and references cited therein).

As can be seen from Eq. (8) the second moment (the variance of the barrier distribution) is proportional to the green-shaded area in Fig. 1. Similarly, the third moment (the skewness) from Eq. (9) is proportional to the integral over the same green-shaded area weighted with the factor $(E - V_C)$ which is positive above and negative below V_C.

Contrary to the analysis of the second derivative, the momentum method does not require fusion excitation functions measured in small energy steps. In order to show this we have used the cross sections measured for the system ^{40}Ca + ^{96}Zr in Ref. [12, 13]. In Table I we present the results of the first four moments by using all, every other, every third *etc.* data point, respectively. The results of these analyses generally agree with each other within two standard deviations. Significant deviations are only observed for the highest moment M_3 when not enough data points are measured in the critical green-shaded area shown in Fig. 1.

III. III. MOMENT ANALYSIS OF FUSION BARRIER DISTRIBUTIONS

In this chapter we discuss values of the moments obtained from experimental data of excitation functions taken from the literature. The comparison is sometimes complicated by the fact that the uncertainties are large or the data differ among the various experiments. One example is the well-known system ^{58}Ni + ^{64}Ni where data from four different groups exist which disagree especially at higher energies [14–17]. It is therefore not always possible to quote uncertainties for all the moment values.

The results are shown in Table II where we have summarized the fusion radius R calculated from the zeroth moment M_0 and the moments M_1, M_2 and M_3 for 26 systems ranging from ^{32}S + ^{48}Ca to ^{16}O + ^{186}W. Also included are the results of R_w, V_w and $\hbar\omega$ (parameters which are equivalent to R, M_1 and M_2), taken from a least-squares fit to the experimental data with the Wong formula (using Eq. (9) of Ref. [34] in the energy region where the fusion cross sections are in the mb range and above) and the radius R_b and the potential barrier V_b obtained from the Akyüz-Winther potential [35].

A. A. Influence of transfer on the fusion radius R

The fusion radius R, calculated from the zeroth moment of the barrier distributions, shows an interesting feature which, to our knowledge, has not been discussed previously. Systems with the largest sub-barrier fusion enhancement in a group with the same Z_1, Z_2 are marked by an asterisk in Table II. In most cases these are systems with a neutron-poor projectile bombarding a neutron-rich target and are always correlated with a small R. This can be seen from a comparison of $E\sigma$ for the Ca + Ca and Ca + Zr systems shown in Fig. 2. The three straight lines in each sub-figure are least-squares fits of Eq. (4) to the data at high energies with the slopes giving the values of πR^2. We observe that the slopes are smallest for the systems ^{40}Ca + ^{48}Ca or ^{40}Ca + ^{96}Zr (black circles in Fig. 2). Since these systems exhibit large transfer cross sections, the fusion yield at high energies is suppressed due to the competition with transfer reactions resulting in a smaller value of πR^2.

Since the values of πR^2 are obtained from experimental data taken at higher energies where the fusion cross sections are large, candidates for the largest fusion enhancement in a group with the same Z_1, Z_2 can be easily identified before starting the time-consuming measurements at sub-barrier energies.

B. B. First and second moments

Extracting values for the first moment (the Coulomb barrier) from excitation functions using Eq.(4) has been done for many years [10]. As can be seen from Table II, the uncertainties of the barriers are typically 1% and the values are in good agreement with the Coulomb barrier V_w obtained from a fit to the data using the Wong model. Deviations are observed mainly for systems which show strong contributions from transfer reactions or where different data sets exist in the literature (e.g. ^{58}Ni + ^{64}Ni).

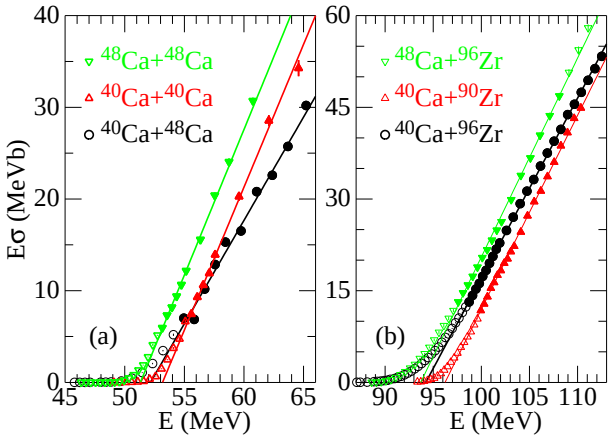

FIG. 2: (Color online) Plots of $E\sigma$ vs E for the fusion systems Ca + Ca and Ca + Zr. The straight lines are least-squares fits of Eq. (4) to the data at high energies (solid circles). The slopes of these lines determine the values πR^2 for each system.

The second moment, M_2, determines the variance of the barrier distribution. It can be seen from Table II that systems with a large fusion enhancement due to transfer reactions not only have a small R but also a large second moment M_2, *i.e.* a wide, sometimes structured barrier distribution $D(E)$.

This correlation is shown in more detail in Fig. 3, where the values of $R - R_{ref}$ are plotted as a function of $\sqrt{M_2}$, where $R_{ref} = 1.2(A_1^{1/3} + A_2^{1/3})fm$. The dashed lines connect systems with the same Z_1, Z_2 but different A_1, A_2. Systems exhibiting the largest fusion enhancements within a group are shown as solid points while the others are shown as open symbols. In this plot all solid points have the largest M_2 and the smallest R within the same group.

A similar isotopic dependence of the width of the barrier distribution has also been observed previously for the Zr + Zr system [36] where the distribution for ^{90}Zr + ^{90}Zr was found to be much smaller than the one for ^{90}Zr + ^{96}Zr.

C. C. Influence of deformation

Higher moments can be extracted from the data as well, but with increasing uncertainties. Values of the third moment M_3 are included in Table II with values ranging from -8 to +152 MeV^3. The large positive values of M_3 observed for some systems, *e.g.* ^{40}Ca + ^{64}Ni, are caused by the long tails on the high energy sides of the

TABLE II: The fusion radius parameter R and the moments $M_1 = V_C$, M_2 and M_3 of the experimental fusion-barrier distributions for a number of heavy-ion fusion systems. R, V_C and their uncertainties originate from least-squares fits using Eq. (4), while M_2, M_3 and their uncertainties result from the integrals given in Eqs. (8) and (9). The uncertainties of the fusion cross section were taken from the literature. The parameters R_w, V_w and $\hbar\omega$ are obtained from fits to the excitation functions with the Wong formula. The radius R_b and Coulomb barrier V_b obtained from the Akyüz-Winther potential [35] are also included.

system	R	M_1	M_2	M_3	R_w	V_w	$\hbar\omega$	$\frac{\sqrt{M_2}}{0.289\hbar\omega}$	R_b	V_b	Ref.
	fm	MeV	MeV^2	MeV^3	fm	MeV	MeV		fm	MeV	
^{40}Ca + ^{40}Ca	9.96 ±0.10	53.17 ±0.07	1.9 ±0.4	2.1 ±1.1	9.74	53.0	3.55	1.3	9.74	54.9	[18]
* ^{40}Ca + ^{48}Ca	8.47 ±0.06	52.16 ±0.05	4.5 ±0.3	6.8 ±1.2	8.13	51.6	4.82	1.5	10.1	53.2	[19]
^{48}Ca + ^{48}Ca	10.04 ±0.05	51.30 ±0.03	1.6 ±0.1	0.9 ±0.2	9.61	51.0	3.23	1.4	10.4	51.7	[20]
^{40}Ca + ^{90}Zr	10.05 ±0.02	96.23 ±0.03	2.5 ±0.2	-0.9 ±1.0	9.94	96.1	5.37	1.0	10.8	99.6	[12]
* ^{40}Ca + ^{96}Zr	9.72 ±0.02	94.28 ±0.02	9.1 ±0.3	-4.7 ±1.1	9.57	94.1	10.1	1.0	10.9	3 98.3	[12, 13]
^{48}Ca + ^{96}Zr	10.01 ±0.04	93.51 ±0.05	7.5 ±0.4	3.0 ±0.9	10.0	93.1	8.91	1.1	11.2	95.9	[21]
^{32}S + ^{90}Zr	11.83 ±0.06	81.81 ± 0.10	21 ±1.4	37 ±7	10.3	79.3	8.50	1.9	10.6	81.2	[22]
* ^{32}S + ^{96}Zr	11.22 ±0.16	80.33 ±0.24	26 ±4	22 ±25	10.1	78.4	12.5	1.4	10.7	80.1	[22]
^{36}S + ^{90}Zr	11.70 ±0.08	77.86 ±0.09	4.6 ±0.7	6.1 ± 2.2	11.1	77.1	4.49	1.7	10.8	79.8	[23]
^{36}S + ^{96}Zr	11.52 ±0.04	75.43 ±0.05	3.1 ±0.3	-1.2 ±0.8	11.2	75.1	4.98	1.2	10.9	78.9	[23]
^{58}Ni + ^{58}Ni	8.34 ±0.27	98.31 ±0.12	4.8 ±0.7	-7.1 ±2.1	7.80	97.8	7.45	1.0	10.6	99.4	[24]
* ^{58}Ni + ^{64}Ni	7.51 ±0.41	98.89 ±0.39	37 ± 11	73 ± 124	7.14	95.3	8.80	2.4	10.8	97.7	[14–17]
* ^{32}S + ^{110}Pd	8.69 ±0.07	87.18 ± 0.06	9.1 ±0.7	-4.7 ±2.7	7.81	86.2	8.83	1.2	10.9	90.5	[25]
^{36}S + ^{110}Pd	8.70 ±0.03	86.35 ±0.03	6.3 ±0.3	0.2 ±1.2	8.23	85.7	7.08	1.2	11.1	89.2	[25]
* ^{32}S + ^{48}Ca	9.34 ±0.09	43.95 ±0.09	7.2 ±0.8	6.9 ±3.1	8.34	42.6	4.88	1.9	9.92	43.3	[26]
^{36}S + ^{48}Ca	10.26 ±0.14	42.51 ±0.19	4.7 ±1.9	23 ±12	9.90	41.8	3.25	2.3	10.1	42.5	[27]
^{40}Ca + ^{58}Ni	9.04 ±0.08	72.14 ±0.08	5.8 ±0.6	10 ±3	8.35	71.1	4.29	2.0	10.2	73.8	[28]
* ^{40}Ca + ^{64}Ni	8.86 ±0.12	70.46 ±0.22	18 ±4	152 ±48	8.29	69.0	5.57	2.6	10.4	72.5	[28]
^{32}S + ^{58}Ni	9.87 ±0.46	59.80 ±0.34	2.8 ±2.5	3 ±12	8.01	59.1	3.50	1.6	9.95	60.2	[29]
* ^{32}S + ^{64}Ni	9.86 ±0.54	57.90 ±0.22	2.9 ±0.9	-1.7 ±1.8	7.76	56.8	4.07	1.4	10.2	59.1	[29]
^{36}S + ^{64}Ni	9.91 ±0.05	56.43 ±0.06	2.2 ±0.3	2.9 ±1.2	9.45	55.9	3.21	1.6	10.3	58.1	[30]
^{16}O + ^{144}Sm	10.63 ±0.02	60.91 ±0.02	4.3 ±0.2	5.2 ±0.5	10.3	60.5	5.71	1.3	10.8	61.7	[31]
^{16}O + ^{148}Sm	10.61 ±0.05	59.81 ±0.05	4.6 ±0.3	-3.0 ±1.0	10.5	59.8	7.88	0.94	10.9	61.3	[31]
^{16}O + ^{154}Sm	10.26 ±0.06	58.93 ±0.05	5.4 ±0.3	-8.0 ±0.8					11.0	60.8	[31, 32]
^{28}Si + ^{154}Sm	9.72 ±0.42	99.41 ±0.49	16 ±5	-8 ±16					11.4	102.6	[33]
^{16}O + ^{186}W	10.68 ±0.04	68.47 ±0.04	6.2 ±0.3	-0.1 ± 1.2					11.4	70.4	[31]

distributions, which, however, have large uncertainties. Fig. 4 presents a plot of the ratio M_3/M_2 as function of $\sqrt{M_2}$.

In the following we will restrict the discussion of M_3 to systems involving spherical ^{16}O ions bombarding various deformed nuclei. The system ^{16}O + ^{154}Sm is a prime example for a system with negative skewness. As discussed in Ref. [31] the deformation of ^{154}Sm leads to a barrier distribution with two limiting situations where ^{16}O approaches the "pole" of the deformed ^{154}Sm or its equator. That is, it leads to a distribution with a peak above the mean and a tail towards lower energies. This structure is well reproduced in the moment analysis of the O + Sm systems. The values of M_3 are negative for ^{154}Sm and positive for the spherical ^{144}Sm. An interesting effect of higher order (β_4) deformations can be observed for the ^{16}O + ^{186}W system. ^{154}Sm has a positive hexadecapole deformation giving from the moment analysis the most negative third moment ($M_3 = (-8.0 \pm 0.8)$ MeV^3). For ^{186}W, however, the β_4 value is negative producing a reduced effective deformation. This leads to a more symmetric barrier distribution [31, 32] and, thus, a small M_3 (-0.1 ± 1.2) MeV^3. (See also Fig. 4).

D. D. Experiments with radioactive beams

As mentioned in section II the moments of the barrier distribution can be obtained from excitation functions which have been measured in larger energy steps. A prime example are systems involving radioactive beams. Beam intensities at existing radioactive beam facilities are 4-5 orders of magnitude below the ones available at accelerators with stable ion beams. For that reason the fusion excitation functions for systems involving radioactive beams have so far been measured in very large energy

TABLE III: The radius parameter R and the moments $M_1 = V_C$, M_2 and M_3 of the experimental fusion-barrier distributions together with their uncertainties for a number of systems with radio-active beams.

system	number of data	R	M_1	M_2	M_3	Ref.
		fm	MeV	MeV^2	MeV^3	
^{6}He + ^{209}Bi	9	10.97 ±0.94	21.18 ±0.93	11 ±9	21 ± 20	[37]
^{15}C + ^{232}Th	5	12.48 ±0.59	64.35 ±0.99	12 ±11	126 ±72	[38]
^{58}Ni+ ^{132}Sn	10	10.93 ±0.58	158.3 ±1.2	13 ±22	118 ±247	[39]

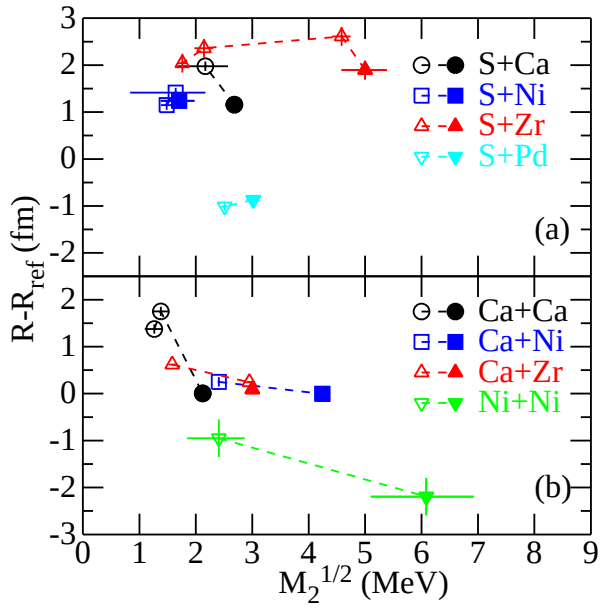

FIG. 3: (Color online) Plots of $R-R_{ref}$ vs $\sqrt{M_2}$ for S-induced (a), and Ca, Ni induced (b) fusion reactions listed in Table II (the results for O, Si + Sm and O + W are not included). Systems with the same Z_1, Z_2 are connected by dashed lines. Systems which exhibit strong transfer reactions are shown by solid points (see text for details).

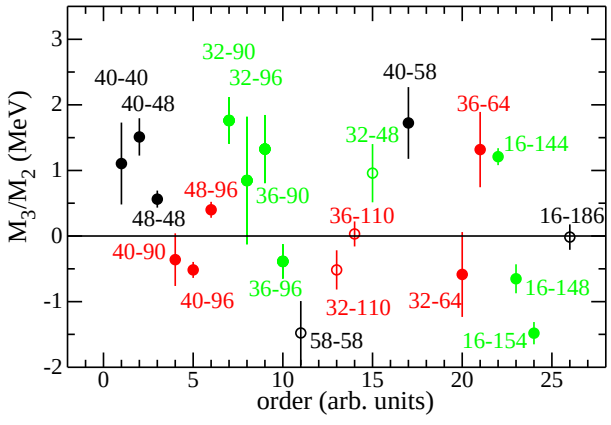

FIG. 4: (Color online) Plot of M_3/M_2, for systems where the uncertainties allow the calculation of a meaningful value of (M_3/M_2). The x-axis is the order in which the systems are quoted in Table II.

steps preventing the extraction of barrier distributions. In addition, the uncertainties of these fusion cross sections are typically 10% or more and, as mentioned in Ref. [1], data from different experiments sometimes disagree in the quoted cross sections.

In this section we discuss a few results of fusion excitation functions with radioactive beams ranging from ^{6}He + ^{209}Bi [37] to ^{58}Ni + ^{132}Sn [39]. Excitation functions of these systems have been measured in the cross section range from $\sim$ 4 to 1000 mb at typically 5-10 energies with uncertainties ranging from 3% to 30%. Plots of $E\sigma$ vs E for two of these experiments are shown in Fig. 5 and the results of the moment analysis are summarized in Table III. While the results from these experiments have large uncertainties especially for the higher moments, the trend of the data again shows large values of M_2 in agreement with the expectations. Future experiments at next-generation facilities will lead to considerable improvements of these values.

E. E. Limitations and future improvements

As mentioned earlier in this paper, the moment method is not affected by the large uncertainties of the second derivatives $\frac{d^2(E\sigma)}{dE^2}$ which are encountered especially at higher bombarding energies. The method, however, assumes that at these energies $E\sigma$ follows a linear dependence, $\pi R^2(E - V_C)$, which is not always the case. It is known that for some systems, *e.g.* ^{12}C + ^{12}C, the cross sections show oscillations due to the reduced number of partial waves contributing to the fusion process [40, 41]. This might affect the values of R and M_1 extracted from the data.

Another point concerns the selection of the upper limit E_h in Eq. (6). While heavy ion fusion cross sections experience a gradual increase towards higher energies the opening of other channels, e.g. incomplete fusion, can lead to a decrease of the fusion yields [42]. This results in a change of the slope of $E\sigma$ at the highest energies. Thus, the upper integration limit E_h needs to be chosen below this energy.

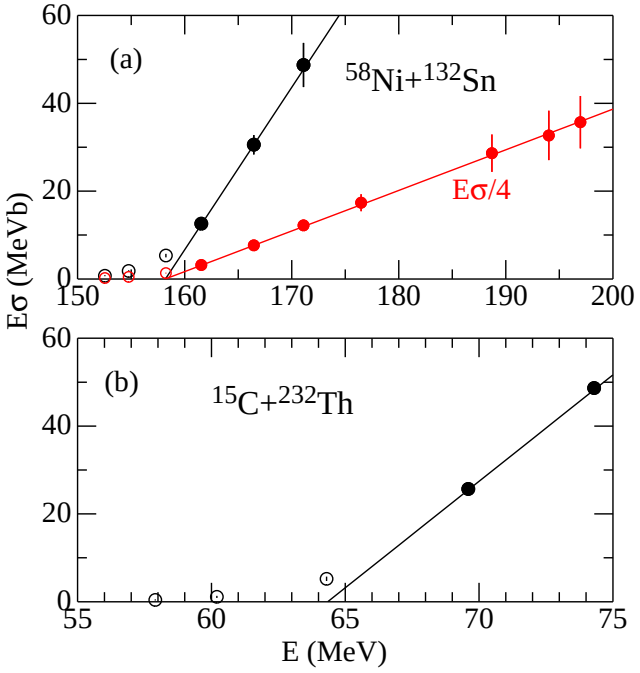

FIG. 5: (color online) Plots of $E\sigma$ vs E for two systems with radioactive beams, (a) ^{58}Ni + ^{132}Sn and (b) ^{15}C + ^{232}Th. The red line and symbols in (a) show the data plotted on a reduced scale. The solid circles are data used in the least-squares fits using Eq. (4).

IV. IV. MOMENTS FROM THE WONG FORMULA AND COUPLED CHANNEL CALCULATIONS

The data summarized in Table II include also parameters obtained from a fit of the data to the Wong formula which corresponds to a barrier distribution for spherical interaction partners. This barrier distribution is given by (Ref. [7, 8, 34]):

$$B_w(E) = (\pi R_w^2)\frac{2\pi}{\hbar\omega}\frac{e^x}{(1+e^x)^2}, \qquad (11)$$

with $x = 2\pi(E - V_w)/\hbar\omega$ and $\int B_w(E)dE = \pi R_w^2$. Here we use the symbols R_w, V_w and $B_w(E)$ to differentiate these values from the ones obtained from the moment method. The barrier distribution defined in Eq. (11) is symmetric with respect to the Coulomb barrier V_w and, thus, cannot describe systems with an asymmetric barrier distribution. As mentioned earlier, the values for the Coulomb barrier V_w are in good agreement with the results obtained from the first moment M_1. For systems with large transfer cross sections the radius R_w shows a similar reduction as observed for the radius R extracted from M_0. Within the Wong model the variance of the barrier distribution, M_2, reflects the quantummechanical transmission through an inverted parabolic barrier, which is related to the curvature of the potential barrier

TABLE IV: Comparison of the parameters R, M_1 and M_2 (column 3, 4, 5) obtained from CC calculations and from experimental data (column 6, 7, 8) for the systems ^{40}Ca + ^{40}Ca and ^{40}Ca + ^{48}Ca.

System	option	R	M_1	M_2	R	M_1	M_2
		fm	MeV	MeV^2	fm	MeV	MeV^2
^{40}Ca+^{40}Ca	ch1	9.51	54.4	0.77			
	inel	9.32	52.9	1.14	9.94	53.1	2.1
* ^{40}Ca+^{48}Ca	ch1	9.80	52.9	0.68			
	tr+inel	8.95	52.4	3.12	8.47	52.2	4.3

$\hbar\omega$ by

$$\sqrt{M_2^w} = 0.289\hbar\omega. \qquad (12)$$

Values of $\sqrt{M_2}/(0.289\hbar\omega)$ are also listed in Table II. While systems with a large fusion enhancement are correlated with large values of $\hbar\omega$ (as pointed out in Ref. [43]), $\hbar\omega$ only partly describes the moment M_2 since $\sqrt{M_2}$ is often greater than $0.289\hbar\omega$. The Wong formula does not supply information for moments M_n with $n > 2$, because it is a single-barrier approximation with only three adjustable parameters.

The moment analysis discussed above has also been applied to coupled-channels calculations. The results of R, M_1 and M_2 obtained from CC calculations [18, 19] are compared in column 3, 4. 5 of Table IV for the two systems, ^{40}Ca + ^{40}Ca and ^{40}Ca + ^{48}Ca. Here, two calculations, ch1 (no coupling) and inel (coupling to inelastic excitation), or ch1 and tr+inel (coupling to transfer reactions and inelastic excitations) are included for the two systems, respectively. The parameters extracted from the experimental data are included in column 6, 7, 8 of Table II for comparison. While channel coupling improves the agreement of the first moment (the Coulomb barrier) and to a lesser extent for the zeroth moment, the width of the barrier distribution increases, but still underpredicts the experimental values.

The radius R_b and the Coulomb barrier V_b obtained from the Akyüz-Winther potential [35] are also included in Table II. For the systems summarized in this table there is a close correlation between the Coulomb barriers extracted from the fusion excitation functions V_C and the Akyüz-Winther potential V_b with an average of 0.981 $\pm$ 0.017 for their respective ratios. A comparison of the fusion radius R and the potential radius R_b, however, shows much larger fluctuations. This is to be expected since R is relatated to the fusion cross sections which show a strong isotopic dependence, while R_b represents the radius of a global nuclear potential which depends only weakly on the mass of the interacting nuclei.

The advantage of obtaining the parameters of the barrier distribution through the moment method can be seen from a comparison of the distributions shown in Fig. 6. The barrier distribution obtained from calculating the second derivative of the energy-weighted cross section using high-statistics data shows that the structure of the

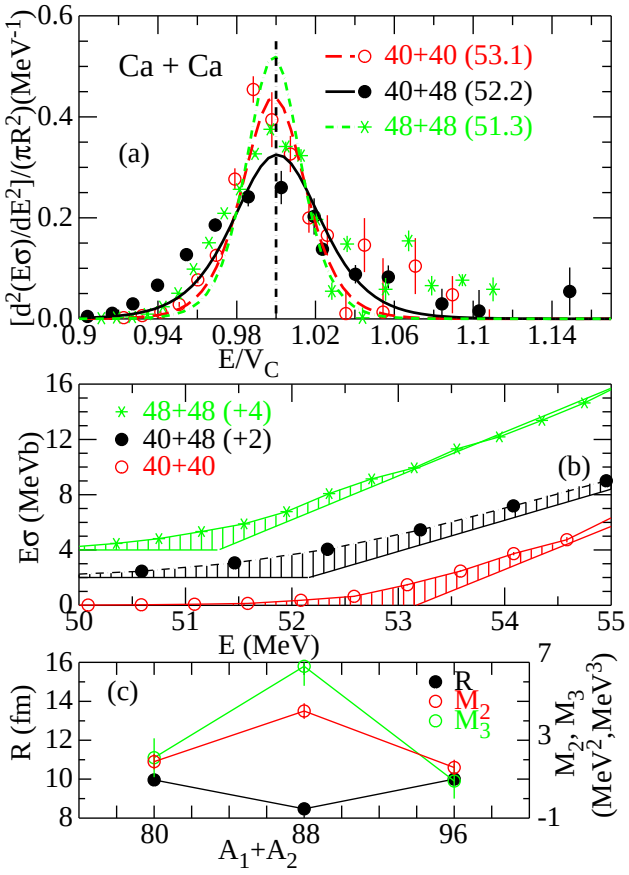

FIG. 6: (Color online) (a): Barrier distributions for three Ca + Ca fusion reactions. The ^{40}Ca + ^{48}Ca system (black) exhibits the widest distribution (large M_2) and the lowest maximum (small R). The symbols are obtained from calculating the second derivative of the energy-weighted, high-statistics cross sections. The curves are the barrier distributions $B_w(E)$ of the Wong model (Eq. (11)). (b): Plot of $E\sigma$ vs E for energies close to the barrier. The second moment M_2 is calculated from the cross-hatched area, which is largest for the ^{40}Ca + ^{48}Ca system shown in black. (c): Plot of R, M_2, M_3 vs $A_1 + A_2$.

distributions for ^{40}Ca + ^{40}Ca and ^{48}Ca + ^{48}Ca are very similar to each other with respect to the maximum and the width, while the barrier distribution for the ^{40}Ca + ^{48}Ca system is broader with a lower maximum corresponding to a larger M_2 and smaller R (see Fig. 6a).

This information can be also obtained from the small slope of the energy-weighted cross sections for system ^{40}Ca + ^{48}Ca shown in Fig. 2a. Similarly, if one compares different systems with the same Z_1, Z_2 using plots like Fig. 1 one observes that the largest deviations of $E\sigma$ from a straight line at energies in the vicinity of the barrier area (the green-shaded area in Fig. 1) are for systems with a large influence of transfer reactions. This is shown for the Ca + Ca system in Fig. 6b where the region around V_C is plotted on an expanded scale. As can be seen from the hatched areas, the ^{40}Ca + ^{48}Ca system shows the largest deviations from a straight line. The moments M_0, M_1 and M_2 for the Ca + Ca reactions are summarized in Fig. 6c, showing again the special nature of ^{40}Ca + ^{48}Ca.

V. V. SUMMARY

In summary, we have introduced a new method to determine the moments, i.e. the average behavior of fusion barrier distributions which can be applied to excitation functions which were measured with large energy steps. The moments of the barrier distributions are obtained directly from the energy-weighted cross sections $E\sigma$ as function of the c.m. energy. The fusion radius R, is obtained from the zeroth moment M_0, *i.e.,* through the slope of energy-weighted cross section $E\sigma$ as function of the energy. The intersection of the extrapolated $E\sigma$ values with the abscissa gives the first moment which is the Coulomb barrier. The second and third moments, the width and skewness of the barrier distribution, are obtained from the area between the energy-weighted experimental cross sections and the ones predicted by the expression $\pi R^2(E - V_C)$. These moments of the barrier distributions are especially useful for a quantitative comparison of different fusion systems.

Such a comparison shows that a large second moment M_2 of the fusion barrier distribution is often correlated with a small fusion radius, which is a strong indication of the influence of transfer reactions on fusion. Negative third moments M_3 for the ^{16}O, ^{28}Si + ^{154}Sm fusion reactions agree with the observation of a strong peak on the high- energy side of the barrier distribution.

VI. ACKNOWLEDGMENT

This work was supported by the US Department of Energy, Office of Science, Office of Nuclear Physics, under Contract No. DE-AC02-06CH11357 and the European Union Seventh Framework Programme FP7/2007-2013 under Grant Agreement No. 262010-ENSAR.

[1] B.B. Back, H. Esbensen, C.L. Jiang, and K.E. Rehm, Rev. Mod. Phys. **86**, 317 (2014).
[2] K. Hagino and N. Takigawa, Prog. Theo. Phys. **128**, 1061 (2012).
[3] C.H. Dasso, S. Landowne, and A. Winther, Nucl. Phys. **A 405,** 381 (1983).
[4] C.H. Dasso, S. Landowne, and A. Winther, Nucl. Phys. **A 407,** 221 (1983).

[5] A.B. Balantekin, S.E. Koonin and J.W. Negele, Phys. Rev. **C 28**, 1565 (1983).
[6] P.H. Stelson, Phys. Lett. **B 205,** 190 (1987).
[7] N. Rowley, G.R. Satchler and P.H. Stelson, Phys. Lett. **B 254,** 25 (1991).
[8] M. Dasgupta, D.J. Hinde, N. Rowley, and A.M. Stefanini, Annu. Rev. Nucl. Part. Sci. **48**, 401 (1998).
[9] H. J. Krappe and H. Rossner, in "Low Energy Nuclear Dynamics" ed. Y. Oganessian et al. World Scientific, Singapore, 1995, p. 329.
[10] R. Bass, Phys. Rev. Lett. **39**, 265 (1977) and Nuclear Reactions with Heavy Ions, Springer Verlag, Berlin, Heidelberg, NewYork, 1980.
[11] A. B. Balantekin, A. J. DeWeerd and S. Kuyucak, Phys. Rev. **C54**, 1853 (1996).
[12] H. Timmers *et al.,* Nucl. Phys. **A 633,** 421 (1998).
[13] A.M. Stefanini *et al.,* Phys. Lett. **B 728,** 639 (2014).
[14] M. Beckerman, M. Salomaa, A. Sperduto, J. D. Molitoris, and A. DiRienzo, Phys. Rev. **C 25**, 837 (1982).
[15] R. Schicker *et al.,* Phys. Lett. **B 206**, 9 (1988).
[16] K.E. Rehm *et al.,* Nucl. Instru. Methods Phys. Res. **A 344**, 614 (1994).
[17] D. Ackermann *et al.,* Nucl. Phys. **A 609**, 91 (1996).
[18] G. Montagnoli *et al.,*, Phys. Rev. **C 85**, 024607 (2012).
[19] C.L. Jiang *et al.,* Phys. Rev. **C 82,** 041601(R) (2010).
[20] A.M. Stefanini *et al.,* Phys. Lett. **B 679,** 95 (2009).
[21] A.M. Stefanini *et al.,* Phys. Rev. **C 73,** 034606 (2006).
[22] H.Q. Zhang *et al.,* Phys. Rev. **C 82**, 054609 (2010).
[23] A.M. Stefanini *et al.,* Phys. Rev. **C 62**, 014601 (2000).
[24] M. Beckerman *et al.,* Phys. Rev. **C 23**, 1581 (1981).
[25] A.M. Stefanini *et al.,* Phys. Rev. **C 52,** 1727(R) (1995).
[26] G. Montagnoli *et al.,* Phys. Rev. **C 87,** 014611 (2013); H. H. Gutbrod *et al.,* Nucl. Phys. **A 213**, 267 (1973).
[27] A. M. Stefanini *et al.,* Phys. Rev. **C 78**, 44607 (2008).
[28] D. Bourgin *et al.,* Phys. Rev.**C 90,** 044610 (2014).
[29] A.M. Stefanini *et al.,* Nucl. Phys. **A 456,** 509 (1986).
[30] G. Montagnoli *et al.,* Phys. Rev. **C 82,** 064609 (2010).
[31] R.G. Stokstad *et al.,* Phys. Rev. Lett. **41**, 281 (1978); Phys. Rev. **C 23**, 281 (1981); J.R. Leigh *et al.,* Phys. Rev. **C 47**, 437 (1993); Phys. Rev. **C 52**, 3151 (1995).
[32] J.X. Wei *et al.,* Phys. Rev. Lett. **67**, 3368 (1991).
[33] S. Gil *et al.,* Phys. Rev. Lett. **65**, 3100 (1990).
[34] C.Y. Wong, Phys. Rev. Lett. **31**, 766 (1973).
[35] A. Winther, Nucl. Phys. **A 594,** 203 (1995).
[36] J. G. Keller *et al.,* Nucl. Phys. **A452,** 173 (1986).
[37] J. J. Kolata *et al.,* Phys. Rev. Lett. **81**, 4580(1998).
[38] M. Alcorta *et al.* Phys. Rev. Lett. **106**, 172701(2011).
[39] Z. Kohley *et al.* Phys. Rev. Lett. **107**, 202701 (2011).
[40] H. Esbensen, Phys. Rev. **C 85**, 064611 (2012) and references therein.
[41] G. Montagnoli *et al.,* Phys. Lett. **B 746,** 300 (2015).
[42] D. Kovar *et al.,* Phys. Rev. **C 20**, 1305 (1979).
[43] C.L. Jiang, K.E. Rehm, B.B. Back, H. Esbensen, R.V.F. Janssens, A.M. Stefanini, and G. Montagnoli, Phys. Rev. **C 89**, 051603(R) (2014).